Spectral hole burning for ultrasound-modulated optical tomography of thick tissue

Xiao Xu*
Sri-Rajasekhar Kothapalli*,†
Honglin Liu
Lihong V. Wang
Washington University in St. Louis
Department of Biomedical Engineering
Optical Imaging Laboratory
St. Louis, Missouri 63130

Abstract. We apply spectral hole burning (SHB)-aided detection in ultrasound-modulated optical tomography (UOT) to image optical heterogeneities in thick tissue-mimicking phantom samples and chicken breast tissue. The efficiency of SHB is improved by using a Tm^{3+}:YAG crystal of higher doping concentration (2.0-atomic%) and a double-pass pumping configuration, in which the pump beam is transmitted through the crystal twice to burn a deeper spectral hole with the available optical intensity. With the improved SHB-UOT system, we image absorbing, scattering, and phase objects that are embedded in the middle plane of a 30-mm-thick phantom sample. The imaging resolution was 0.5 mm in the lateral direction, as defined by the focal width of the ultrasonic transducer, and 1.5 mm in the axial direction, as determined by the ultrasonic burst length. We also image two absorbing objects embedded in a 32-mm-thick chicken breast sample. The results suggest that the improved SHB-UOT system is one step closer to the practical optical imaging application in biological and clinical studies. [DOI: 10.1117/1.3505486]

Keywords: ultrasound-modulated optical tomography; optical imaging; spectral hole burning; scattering medium; diffuse medium.

Paper 10488LR received Sep. 1, 2010; revised manuscript received Sep. 28, 2010; accepted for publication Sep. 29, 2010; published online Dec. 13, 2010; corrected Dec. 16, 2010.

Optical imaging of biological tissue has become an increasingly important tool in biomedical research in recent years. While optical imaging provides excellent optical contrast, it lacks good spatial resolution for thick biological tissues because of the strong light scattering. Various imaging modalities have been explored to overcome this difficulty. Among them, ultrasound-modulated optical tomography (UOT)[1] is a promising hybrid technique capable of imaging both scattering and absorption contrasts.[2] In UOT, a focused ultrasonic beam encodes the diffused coherent light inside a scattering medium by phase modulation. Detection of the ultrasonically encoded (i.e., modulated or tagged) photons enables one to recover the spatial distribution of the diffused photon fluence inside the medium to map optical properties, which are of biomedical interest. Wang, Jacques, and Zhao[1] first experimentally demonstrated UOT by modulating a *cw* laser with a *cw* ultrasound and obtained images of objects embedded in tissue-mimicking phantoms. Leveque et al.[3] improved the signal-to-noise ratio (SNR) of UOT by implementing a parallel detection method, where a charge-coupled device (CCD) camera was used as a detector array with a source-synchronized lock-in technique. Sakadzic and Wang,[4] and Rousseau, Blouin, and Monchalin[5] used pulsed ultrasound modulation and long-cavity Fabry-Perot interferometric detection to obtain microscopic UOT images in biological tissues with imaging resolution scalable to ultrasound wavelength ($<100\ \mu$m) at imaging depths greater than 3 mm. Murray et al.[6] proposed the use of a photorefractive crystal (PRC)-based detection system to enhance detection efficiency. Subsequently, PRC detection for UOT imaging was investigated at near-infrared wavelengths ($\lambda = 1064$ nm) by Ramaz et al.,[7] and used to study the tissue optical and mechanical properties by Xu et al.[8] Theories on the mechanism of ultrasound modulation of diffused light were also developed by various groups.[9–11]

The low signal-to-noise ratio of UOT, however, remains the greatest challenge to implement UOT in biomedical applications. The difficulty comes from several factors. First, the modulation depth, defined as the ratio of the ultrasound-modulated light intensity to the unmodulated light intensity, is low because the ultrasonic focal volume is small compared to the entire light diffusion volume. Secondly, the diffused light has a speckled wavefront as a result of multiple scattering in the turbid medium, which limits detection efficiency. Coherent detection of the modulated light is confined to single speckles to observe maximal modulation depth; otherwise, mixing of the modulated and the unmodulated light at the detector surface further deteriorates the SNR, because the two sets of wavefront speckles follow independent statistics and add up incoherently. In addition, the temporal coherence of the speckles is degraded by speckle decorrelation, which is caused by internal movement of the turbid medium, such as Brownian motion. Spectral hole burning (SHB) was recently proposed[12,13] as a front-end absorptive filter in UOT to improve detection efficiency, which circumvents the spatial and temporal coherence limit in

*Authors contributed equally.
†Current address: Stanford University, Department of Radiology, Molecular Imaging Program at Stanford and Bio-X Program, Palo Alto, California 94305.

Address all correspondence to: Lihong V. Wang, Optical Imaging Laboratory, Department of Biomedical Engineering, Washington University in St. Louis, One Brookings Dr., Campus Box 1097, St. Louis, MO 63130. Tel: 314-935-6152; Fax: 314-935-7448; E-mail: lhwang@biomed.wustl.edu.

1083-3668/2010/15(6)/066018/5/$25.00

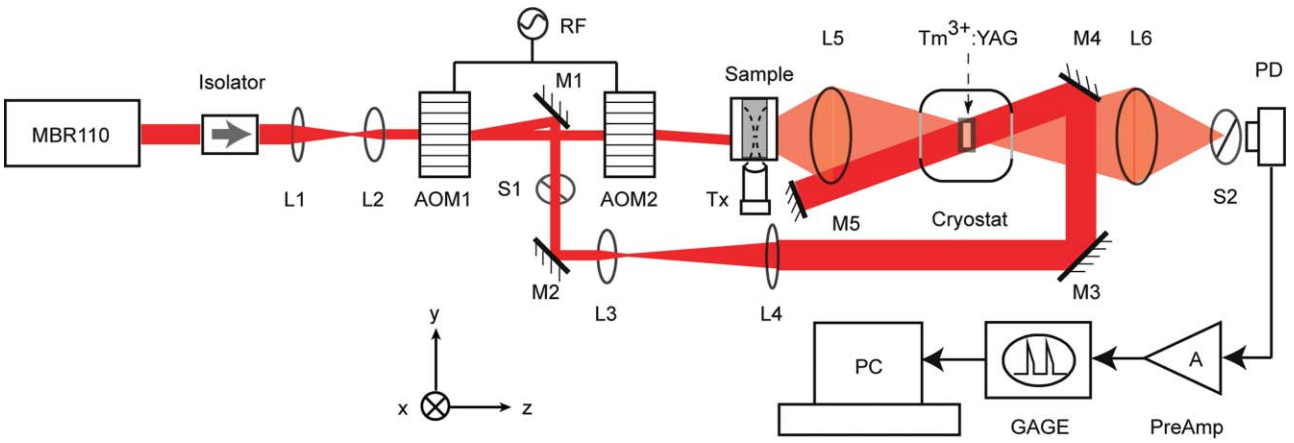

Fig. 1 Schematic of the double-pass SHB-UOT experimental setup. MBR110, cw Ti-sapphire laser; L1 through L6, lenses; M1 through M5, mirrors; AOM1 and AOM2, acousto-optic modulators; rf, AOM controller; S1 and S2, mechanical shutters; Tx, ultrasonic transducer; PD, photodiode; PreAmp, preamplifier; GAGE, 200-MHz data acquisition card; and PC, personal computer.

detecting the speckled wavefront by selectively passing the modulated light while suppressing all of the other spectral components. In the ideal case, all SHB-filtered photons are ultrasonically encoded ones; thus, the speckle grains can be added in terms of intensity, although the filtered wavefront of the modulated light is still speckled. Compared with other detection techniques for UOT, SHB detection has the advantage of a higher etendue, and therefore can detect more modulated light, which becomes increasingly critical in imaging thicker tissues. The applicability of SHB in UOT was experimentally demonstrated with imaging results from 10-mm-thick biological-tissue-mimicking phantom samples.[12,13]

In this work, we report more experimental results as we further explore the potential of SHB for UOT imaging of thicker biological tissue. To improve SHB efficiency, we implemented a double-pass pumping scheme, which resulted in deeper spectral holes with the available pump-beam intensity. The enhanced imaging ability was demonstrated by differentiating the absorbing, scattering, and phase objects in a 30-mm-thick tissue-mimicking phantom with good lateral and axial resolutions. High resolution images of absorbing objects embedded in the middle of 32-mm-thick chicken breast tissue were also obtained. These results advance the SHB-UOT one step closer to optical imaging in biological and clinical studies.

Figure 1 schematically shows our experimental setup for UOT with SHB, whose single-pass version was implemented and described earlier.[12,13] A key component of the system is the SHB material, a 2.0-atomic%-doped Tm^{3+}:YAG crystal. When its temperature is cryogenically cooled below 4.7 K, the crystal shows an absorption peak at $\lambda = 793.38$ nm, corresponding to the $^3H_6 \rightarrow {}^3H_4$ transition of the Tm^{3+} ions.[14,15] Several factors make the Tm^{3+}:YAG crystal an attractive choice of a narrow-band spectral filter for UOT study: its operating wavelength is in the near-infrared (NIR) region, which is a preferred biomedical imaging window; its inhomogeneous absorption linewidth of 25 GHz is broad enough to accommodate clinical ultrasonic frequency; and its homogeneous linewidth of ~150 kHz facilitates effective removal of the unmodulated light. When the crystal is illuminated by a pump beam of a prescribed frequency shift (tuned with AOM1 in Fig. 1), a narrow spectral hole is burned within the absorption band. Within the 10-ms lifetime[15] of the spectral hole, the SHB crystal acts as a narrow-band spectral filter by strongly absorbing spectral components of the signal light that are outside of the engraved spectral hole. Both the pump and the signal light beams are derived from the same source—a cw Ti:sapphire laser (Coherent MBR110E), which is pumped by a frequency-doubled diode pumped Nd:YAG laser [Coherent (Santa Clara, California) Verdi V10] and operates at 793.38 nm with a linewidth of ~181 kHz and output power of 2 W. Two acousto-optic modulators [AOMs, IntraAction (Bellwood, Illinois) AOM 802-A1] work in combination with an ultrasound transducer to match the frequencies of the pump beam and the ultrasound-modulated light on the signal path. In the experiment, AOM1 was first turned on for 3.3 ms with a 70-MHz sinusoidal rf wave, diffracting light into the first order. This first order beam, used as the pump beam, was then expanded into a 9-mm-diam collimated beam delivering 900-mW optical power. After AOM1 was turned off, AOM2 was turned on with a 75-MHz sinusoidal rf wave, diffracting the incident laser beam into its first order to illuminate the scattering sample. The diffused light inside the sample interacted with a traveling ultrasound burst consisting of five cycles of 5-MHz sinusoidal wave, which was emitted by a focused transducer [Panametrics (Waltham, Massachusetts) NDT A326S; focal length 16.2 mm; focal width 0.5 mm]. The interaction generated the ultrasound-modulated component within the signal light exiting the sample. A condensing lens (L5) after the sample then focused the signal light onto the SHB crystal placed inside the cryostat chamber. The modulated component of the signal light was spectrally filtered by the SHB crystal before it was detected by a large area (3.6×3.6 mm^2) photodiode [Thorlabs (Newton, New Jersey) PDA55]. The output signal was fed through a preamplifier [Stanford Research (Sunnyvale, California) SR560] and coupled into a digitizer [Gage (Lockpost, Illnois) CompuScope 14200] for data analysis.

The efficiency of the SHB crystal as a narrow-bandpass filter depends on the depth of the spectral hole. To burn a deeper hole with the available optical power, we used a double-pass pumping scheme, where mirror M5 was placed diagonal to M4 across the cryostat to reflect the pump beam back onto the Tm^{3+}:YAG

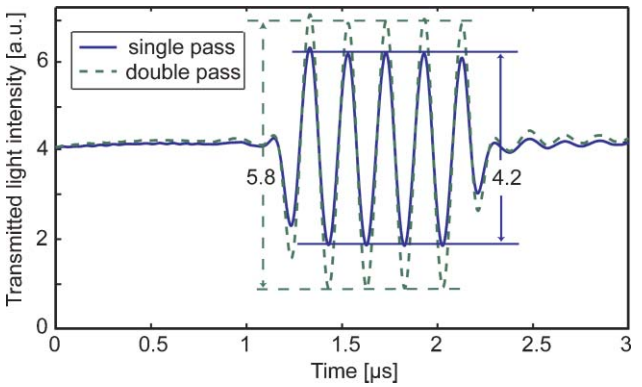

Fig. 2 Comparison of the transmitted probe beam powers. The probe beam was modulated by a five-cycle 5-MHz ultrasound burst and filtered by the SHB crystal, when the SHB is operated in single-pass and double-pass pumping configurations.

crystal. To quantify the increase in the spectral hole depth benefiting from the double-pass pumping scheme compared to the conventional single-pass method, we measured the transmission of a weak probe beam (~15 μW) through the SHB crystal, which was modulated by a five-cycle 5-MHz ultrasound burst when passing through the transducer focus in a clear gelatin phantom. A 38% increase in transmission efficiency was observed (Fig. 2). Assuming the validity of Beer's law $I_{out} = I_{in} \exp(-\alpha_0 \cdot L_C)$, and given $L_C = 2.5$ mm for the thickness of the Tm^{3+}:YAG crystal used in the experiment, we found a reduction of the absorption coefficient $\Delta\alpha_0(\omega_P) = 0.13$ mm^{-1} at pump light frequency ω_P due to the increased spectral hole depth with the double-pass pumping scheme.

Improvement with the double-pass pumping method suggests that it is possible to burn deeper spectral holes if higher optical power is available in the laser. In our experiment, a 2.5-mm-thick, 2.0-atomic%-doped Tm^{3+}:YAG crystal was pumped by a 900-mW beam with a 9-mm collimated beam diameter for 3.3 ms. As a comparison, in a previous demonstration,[14] a 2.5-mm-thick, 0.5-atomic%-doped Tm^{3+}:YAG crystal was used as a spectral filter, which was pumped by laser pulses lasting 150 μs with a typical pulse energy of 450 nJ and a beam waist of 90 μm. The fluence at the crystal surface due to the pump light was 1.5 times as large as that in our experiment. On the other hand, since the doping concentration of our crystal is four times as large, even higher optical power is needed to reach SHB saturation[12] in our experiment. The higher doping concentration of the SHB crystal, while enabling a deeper spectral hole and hence better spectral filtering, comes at the expense of the increased spectral hole width, which turned out to be of negligible consequence for our imaging applications.

In the initial studies of SHB-assisted detection in UOT,[12,13] an imaging experiment was conducted on a 10-mm-thick tissue-mimicking phantom sample. To explore its potential in a practical biomedical imaging setting, it is desirable to use SHB-assisted UOT to image real biological tissues of thicknesses

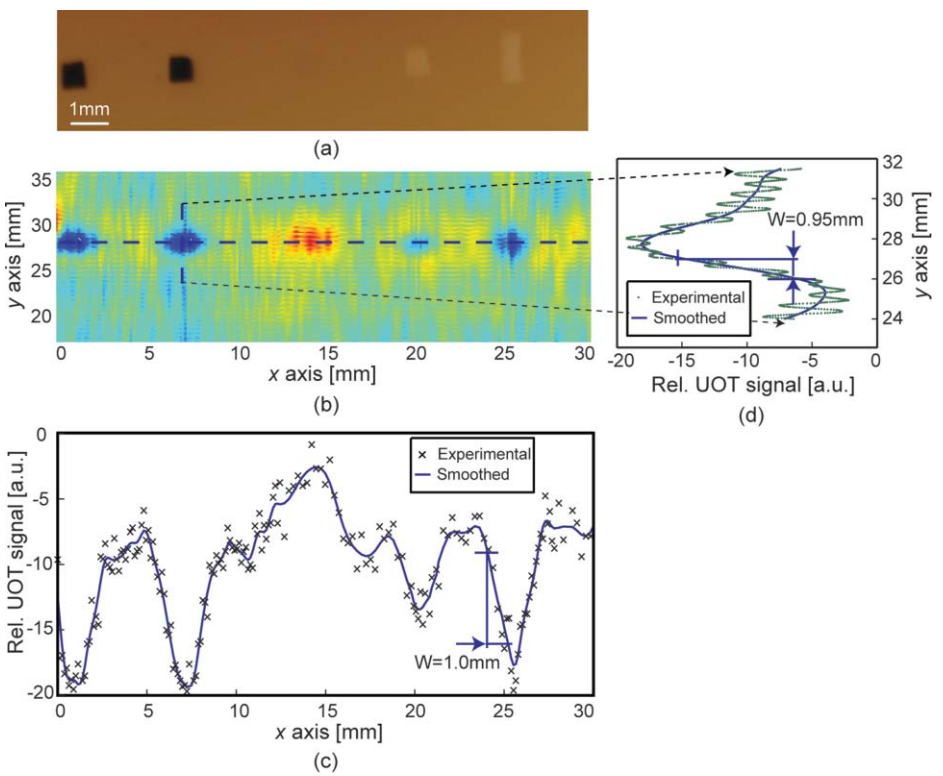

Fig. 3 UOT images of the absorbing, scattering, and phase objects embedded in the middle plane of a 30-mm-thick intralipid phantom slab. (a) A photograph of the intralipid sample with the five embedded objects: two absorbing objects of dimensions 1.5×1.5×1.5 mm^3 on the left; one phase object of 1.5×1.5×1.5 mm^3 in the middle; and two scattering objects of 1.5×1.5×1.5 mm^3 and 2×3×2 mm^3, respectively on the right. (b) A B-scan image of the five objects obtained from SHB-UOT. (c) A 1-D image of the five objects along the B-scan direction, denoted by the horizontal dashed line in (b). (d) An A-scan image of the second absorbing object, denoted by the vertical dashed line in (b). The smoothed curves were obtained by fast Fourier transform (FFT) filtering.

beyond 10 mm. With improved detection efficiency resulting from the double-pass pumping scheme using a higher doping SHB crystal, the deep tissue imaging capability of our SHB-UOT system was put to the test with these objectives in mind. The tissue-mimicking samples were prepared by mixing 10-wt% porcine gelatin [Sigma (Saint Louis, Missouri) G2500] and 1-wt% intralipid (Fresenius Kabi, Hamburg, Germany) in distilled water, and molding the solution into slabs of various thicknesses along the light propagation direction. The light incident side of the sample has the dimension of 100×60 mm^2. The background samples have the reduced scattering coefficient $\mu_s' = 0.7$ mm^{-1} for the laser wavelength 793.38 nm and thickness of 30 mm.

A typical imaging result obtained from the UOT experiment with SHB detection is shown in Fig. 3, which was a reconstructed image of five objects embedded in a 30-mm-thick tissue-mimicking phantom. These objects represent three distinctly different optical heterogeneities commonly encountered in optical imaging of biological tissue: the absorbing objects, the scattering objects, and the phase object—a volume with a uniform refractive index—in a scattering background. The absorbing objects, with the same composition as the background gelatin matrix but dyed with black India ink, have an optical absorption coefficient $\mu_a = 10$ mm^{-1}; the scattering objects, with 3-wt% intralipid added to the gelatin matrix, have a higher reduced scattering coefficient $\mu_s' = 3$ mm^{-1}; the phase object, made from 10-wt% gelatin solution that contains no intralipid, is optically transparent and homogeneous. The objects have dimensions of $1.5\times1.5\times1.5$ mm^3 or $2\times3\times2$ mm^3—much smaller than the ultrasonic focal zone of 16 mm in length. Figure 3(a) is a photograph of the sample, dissected at the middle plane, containing all five objects, and Fig. 3(b) is the B-scan UOT image with SHB detection. Figure 3(c) shows an A-line image of the second absorbing object, corresponding to the vertical dashed line in Fig. 3(b). Figure 3(d) shows a 1-D image of all five objects along the horizontal dashed line in Fig. 3(b). The imaging result of different objects can be explained by the different mechanisms involved in the ultrasonic modulation of the diffused light.[2] On one hand, the decrease of the UOT signal at the site of absorbing objects is due to strong absorption of the diffused photons. On the other hand, the decrease of the signal at the site of higher scattering objects is due to the cancellation of different phase accumulation terms, resulting in reduction in the amplitude of the ultrasound-modulated light. By contrast, ultrasound-modulated light amplitude is increased at the site of lower scattering/clear objects relative to that of the higher scattering background (e.g., phase objects). It is almost intuitive that the lower the scattering coefficient of the object relative to the background, the stronger the UOT signal.[16] It is therefore feasible, in principle, to map the distribution of the scattering coefficient based on the relative changes in UOT signal. The axial and lateral resolutions of the imaging experiment can be quantified from Figs. 3(c) and 3(d). The resolution, defined here as the width between the 20 and 80% rise points on either edge of the object, is 0.95 mm along the acoustical axis and 1.0 mm perpendicular to the acoustical axis. The axial resolution is ~60% of the full spatial extent—1.5 mm—of the five-cycle 5-MHz ultrasound burst, indicating good agreement between the experimental measurement and the theoretical expectation. The lateral resolution appears larger than the ultrasonic focal width as a result of the convolution of the ultrasonic focus and the

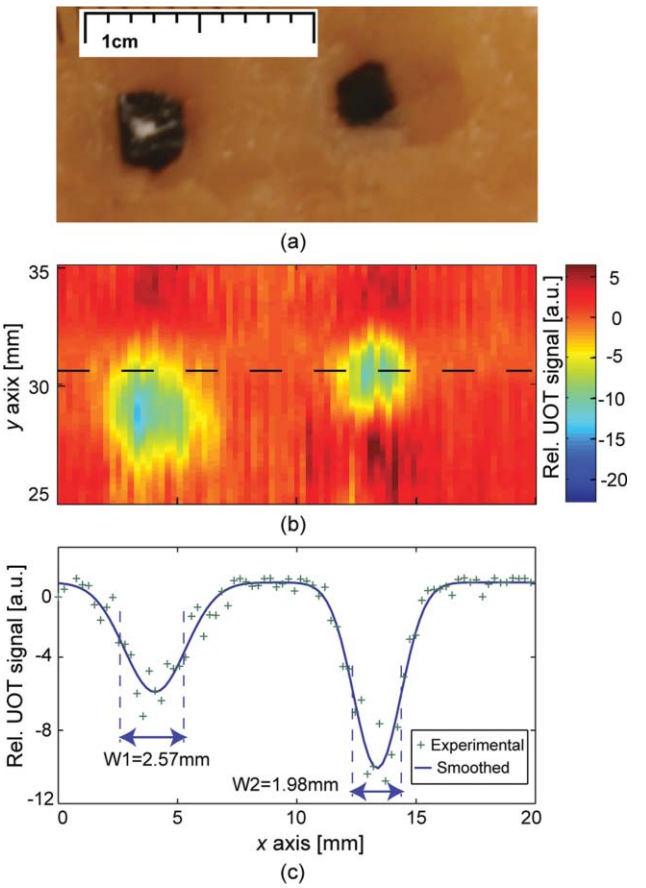

Fig. 4 UOT images of a 32-mm-thick chicken breast sample. (a) Photograph of the sample embedded with two absorbing objects of absorption coefficient $\mu_a = 10$ mm^{-1} and dimensions $3\times3\times3$ mm^3 and $2\times2\times2$ mm^3, respectively. (b) A B-scan image of the sample. (c) A 1-D image of the two objects along the B-scan direction, denoted by the horizontal dashed line (smoothed over the experimental data points) in (b). The smoothed curve was obtained by FFT filtering.

imaging object. This result clearly demonstrates the sensitivity of the technique for imaging all three types of objects of approximate millimeter dimensions in the 30-mm deep tissue regime. Especially notable is the axial resolution in imaging scattering objects in comparison with the previous study,[2] where UOT was first shown to image scattering objects ($2\times2\times20$ mm^3) that occupied the entire length (20 mm) of the ultrasonic focal zone.

Finally, to demonstrate the feasibility of SHB-UOT for deep tissue imaging in real biological samples, a 32-mm-thick chicken breast sample was imaged. Two small absorbing objects, made with the same composition as the imaging objects in Fig. 3, were embedded 10 mm apart in the middle plane of the sample. The result is shown in Fig. 4. The full widths at half maxima of the imaged objects, quantified from Fig. 4(c), are 2.6 and 2.0 mm, respectively, and agree well with the real dimensions of the objects. The high signal-to-noise ratio (SNR), resulting from the improved SHB detection in UOT, makes a prominent distinction between the absorbing objects and the tissue background, which verifies its potential in biomedical imaging applications such as breast cancer screening.

In summary, SHB-UOT's high-resolution, deep imaging ability in biological tissue is experimentally demonstrated. Its ability in distinguishing both optically scattering and absorbing

heterogeneities from the background tissue is verified. Currently, the burned spectral hole is far from saturation because of the limited optical pump power available in the laser. Also, the finite size of the optical window of the cryostat is the only factor limiting the achievable etendue in detection of the diffused light. Our double-pass experiment results suggest that by increasing the optical pump power and optical window size of the cryostat, further improvements can be made to exploit the full potential of the SHB detection for UOT, and push its capacity toward small animal imaging and clinical diagnostic imaging.

Acknowledgment

We are thankful to Chulhong Kim for his assistance with an early system setup. This research is funded in part by the National Institutes of Health grants R01 EB000712 and U54 CA136398.

References

1. L. V. Wang, S. L. Jacques, and X. M. Zhao, "Continuous-wave ultrasonic modulation of scattered laser-light to image objects in turbid media," *Opt. Lett.* **20**, 629–631 (1995).
2. S. R. Kothapalli, S. Sakadzic, C. H. Kim, and L. V. Wang, "Imaging optically scattering objects with ultrasound-modulated optical tomography," *Opt. Lett.* **32**, 2351–2353 (2007).
3. S. Leveque, A. C. Boccara, M. Lebec, and H. Saint-Jalmes, "Ultrasonic tagging of photon paths in scattering media: parallel speckle modulation processing," *Opt. Lett.* **24**, 181–183 (1999).
4. S. Sakadzic and L. V. Wang, "High-resolution ultrasound-modulated optical tomography in biological tissues," *Opt. Lett.* **29**, 2770–2772 (2004).
5. G. Rousseau, A. Blouin, and J. P. Monchalin, "Ultrasound-modulated optical imaging using a high-power pulsed laser and a double-pass confocal Fabry-Perot interferometer," *Opt. Lett.* **34**, 3445–3447 (2009).
6. T. W. Murray, L. Sui, G. Maguluri, R. A. Roy, A. Nieva, F. Blonigen, and C. A. DiMarzio, "Detection of ultrasound-modulated photons in diffuse media using the photorefractive effect," *Opt. Lett.* **29**, 2509–2511 (2004).
7. F. Ramaz, B. C. Forget, M. Atlan, A. C. Boccara, M. Gross, P. Delaye, and G. Roosen, "Photorefractive detection of tagged photons in ultrasound modulated optical tomography of thick biological tissues," *Opt. Exp.* **12**, 5469–5474 (2004).
8. X. Xu, H. L. Zhang, P. Hemmer, D. K. Qing, C. H. Kim, and L. V. Wang, "Photorefractive detection of tissue optical and mechanical properties by ultrasound modulated optical tomography," *Opt. Lett.* **32**, 656–658 (2007).
9. W. Leutz and G. Maret, "Ultrasonic modulation of multiply scattered-light," *Physica B* **204**, 14–19 (1995).
10. L. V. Wang, "Mechanisms of ultrasonic modulation of multiply scattered coherent light: an analytic model," *Phys. Rev. Lett.* **87**(4), 043903 (2001).
11. S. Sakadzic and L. V. Wang, "Correlation transfer and diffusion of ultrasound-modulated multiply scattered light," *Phys. Rev. Lett.* **96**(16), 163902 (2006).
12. Y. Z. Li, P. Hemmer, C. H. Kim, H. L. Zhang, and L. V. Wang, "Detection of ultrasound-modulated diffuse photons using spectral-hole burning," *Opt. Exp.* **16**, 14862–14874 (2008).
13. Y. Z. Li, H. L. Zhang, C. H. Kim, K. H. Wagner, P. Hemmer, and L. V. Wang, "Pulsed ultrasound-modulated optical tomography using spectral-hole burning as a narrowband spectral filter," *App. Phys. Lett.* **93**, 011111 (2008).
14. G. Gorju, V. Crozatier, I. Lorgere, J. L. Le Gouet, and F. Bretenaker, "10-GHz bandwidth RF spectral analyzer with MHz resolution based on spectral hole burning in Tm3 + :YAG," *IEEE Photon. Tech. Lett.* **17**, 2385–2387 (2005).
15. L. Menager, I. Lorgere, J. L. Le Gouet, D. Dolfi, and J. P. Huignard, "Demonstration of a radio-frequency spectrum analyzer based on spectral hole burning," *Opt. Lett.* **26**, 1245–1247 (2001).
16. S. R. Kothapalli, S. Sakadzic, C. H. Kim, and L. V. Wang, "Imaging of optical scattering contrast using ultrasound-modulated optical tomography," *Proc. SPIE* **6856**, 68561p (2008).